*Astronomical Data Analysis Software and Systems IV*
*ASP Conference Series, Vol. 77, 1995*
*R. A. Shaw, H. E. Payne, and J. J. E. Hayes, eds.*

# Modelling Astrophysical Turbulent Convection

N. Brummell and J. Toomre

*Joint Institute for Laboratory Astrophysics, Department of Astrophysical, Planetary and Atmospheric Sciences, University of Colorado, Boulder, CO 80309-0440*

**Abstract.** Numerical simulations of highly turbulent flows in astrophysics benefit greatly from recent advances in high performance computing. Yet such three-dimensional modelling raises major problems in capturing, moving, and analyzing the resulting massive data sets necessary to sample the evolving intricate dynamics. Thus archiving, networking, and visualization are as essential as the actual act of computing when it comes to real scientific progress.

## 1. Introduction

An interdisciplinary team of researchers at several institutions (Universities of Colorado, Chicago, and Minnesota, Michigan State University, and National Center for Atmospheric Research) is working jointly on problems in geophysical and astrophysical fluid dynamics (GAFD) to utilize massively-parallel architectures to increase the spatial resolution in three-dimensional simulations of GAFD turbulence. Within our "grand challenge" team efforts, we are employing variously pseudo-spectral, finite-difference, multi-grid, and piecewise-parabolic method (PPM) approaches in studying the intense turbulence encountered in both planetary and stellar settings. The scale of these simulations requires corresponding progress in the computational sciences, both in order to develop and optimize software for massively-parallel computers and to capture and visualize the resulting massive data sets.

Our research related to astrophysics has so far concentrated largely on turbulent compressible convection within stars. In particular, the vigorous turbulence that results from convective instability within rotating stars not only serves to transport heat but also to redistribute angular momentum and chemical species, and can yield magnetic dynamo action. A hallmark of such turbulence constrained by rotation and stratification is that *large-scale coherent structures and strong mean flows can coexist with the intense smaller-scale turbulence.* Our work with three-dimensional direct simulations of turbulent compressible convection influenced by rotation is motivated by trying to understand how stars and giant planets rotate differentially, and in particular to examine the redistribution of angular momentum that leads to differential rotation within a star like the sun. As one example, these studies seek to resolve a major challenge raised recently by helioseismology, wherein acoustic oscillations of the sun are used to probe the structure and dynamics of the solar convection zone. Preliminary results from helioseismology (cf. Gough & Toomre 1991) suggest that the sun is rotating differentially with depth and latitude in a manner very different from predictions based on earlier numerical simulations. Those spherical shell simulations of rotating anelastic convection (e.g., Gilman & Miller 1986; Glatzmaier 1987) dealt with effectively laminar convective flows, whereas our recent work suggests that *fully turbulent* compressible flows appear to yield very different transport properties for angular momentum. This holds out the hope that in due course simulations of GAFD turbulence carried out in appropriate spherical geometries and with the inclusion of adequate stellar physics (realistic equations of state and opacities, ionization effects) may help to resolve the basic dynamical puzzle now being raised by helioseismology. However, understanding such nonlinear dynamics at a fundamental level raises formidable challenges because of the broad range of physical scales that must be resolved. High-performance computing offers the opportunity to make substantial inroads for studying the properties of such astrophysical turbulence.

## 2. Profile of Turbulence Simulations

The basic difficulty with trying to model turbulence in most natural settings, and certainly so in a stellar convection zone, is that the active dynamical scales of convection encompass a formidable range. Turning to the sun, we expect that the largest-scale turbulent flows deep within the convection zone should possess scales comparable to the overall depth of that zone (occupying the outer 30 percent by radius, or about 200,000 km in depth). Yet the density scale height near the top of the zone is only about 100 km, and one readily observes there intense turbulent convection in the form of granulation with horizontal scales of order 1,000 km. Detectable there, too, are supergranulation flow patterns with scales of order 30,000 km. However, we can estimate that viscous dissipation is operating at scales of order 0.1 km or smaller, suggesting that the active dynamical scales of turbulence in such a zone range at least from $10^5$ to $10^{-1}$ km, or thus over six decades in each physical dimension. The most intricate three-dimensional turbulence simulations to date have just begun dealing with order $1024^3$ spatial modes, capturing three decades in each dimension. As we will discuss below, such $10^9$ spatial zone calculations to study the evolution of turbulence for typically $10^5$ time steps make rather interesting demands on processors, memory, communications, and data capture. Though we may have to wait for quite some time before $10^{18}$ zone simulations become tractable (if ever), we can take some comfort in realizing that the hints of structured turbulence first realized with $128^3$ simulations are now seen in fascinating detail with the $1024^3$ "hero" calculations of the day. Another three decades of resolution (and degrees of freedom) in each physical dimension may well herald other surprises in the resulting turbulent dynamics. The optimism of theoretical physics encourages great extrapolations to be made, and in that spirit we hope that the turbulence calculations of $4096^3$-class likely by the end of this decade and century may provide substantial clues about the inner workings of a real star like the sun. Yet we recognize that all such modelling is of the large-eddy simulation (LES) variety, requiring some manner of sub-grid-scale (SGS) representation of the unresolved scales.

### 2.1. Memory Requirements and Operation Counts

The nature of our computational challenges are revealed by considering some of the attributes of a $1024^3$-mode turbulence simulation. For fully compressible convection, we typically use as working variables the three components of velocity $(u, v, w)$, pressure $p$, and temperature $T$. This implies that the memory requirements are 160 GB, based on $10^9$ spatial zones $\times$ 5 variables $\times$ factor 4 of working space, for a total of about 20 Gwords. On a 1024-node massively parallel processor (mpp) system, we effectively need 160 MB of memory per node. Turning to estimates of operation counts for these simulations, the floating point operation (flop) count per zone per time step range from about 200 for pseudo-spectral codes to about 4000 for PPM codes. Since the intricate dynamics needs to be evolved for about 100,000 times steps, the total operation count for a given simulation are $2 \times 10^{16}$ flop using pseudo-spectral codes and $4 \times 10^{17}$ flop using PPM codes. Once a real Tflop $\mathrm{s}^{-1}$ machine (1000 Gflop $\mathrm{s}^{-1}$) is realized, such a pseudo-spectral run could be accomplished in $2 \times 10^4$ s (about 6 hours), whereas the PPM run requires $4 \times 10^5$ s (about 110 hours). At the sustained 20 Gflop $\mathrm{s}^{-1}$ that is about the best performance now, these numbers translate into $10^6$ s (280 hours) and $2 \times 10^7$ s (5500 hours).

### 2.2. Data Flow and Data Capture

The choice of computational fluid dynamics algorithms to be favored on a given mpp architecture is considerably influenced by the effective internal communication speed between processors. The use of fully explicit and spatially local methods, such as PPM, places the least demands on such communication. With PPM, our 3–D simulations on regular grids can be subdivided into many subvolumes, with only values of variables on boundary zones a few layers deep having to be exchanged after each time step between processors working on adjacent subvolumes. If the operation count is high, this is a relatively infrequent event. In contrast, pseudo-spectral codes assign successive physical planes to the processors, and carry out fast transforms on these planes within processors, followed by data transposes when calculations are required in the final dimension. Alternatively, the transforms may be carried out in parallel across processors, with either approach requiring fairly intensive data movement. Since the operation counts with pseudo-spectral codes are typically far more modest than with PPM, communication currently places major constraints upon the actual performance realized with the principal mpp contenders.

Of greater concern is how to extract and capture sufficient data to be used for subsequent visualization and analysis of these intricate turbulent flows. A single data snapshot of five fields and two tracers at $1024^3$-resolution yields 56 GB per dump. If we sample the time evolution fairly sparsely after every 100 time steps (or $10^3$ samples per run), then the full data set is about 56 TB per run. Not only is that number rather large given most current mass storage facilities, but the data flow rate will also be problematic as the computing machines get faster. On current 20 Gflop $\mathrm{s}^{-1}$ machines, the required data outflow for the PPM code is a tractable 2.8 MB $\mathrm{s}^{-1}$, and for the pseudo-spectral code (with about 20-fold fewer operations per time step) a more difficult 56 MB $\mathrm{s}^{-1}$. Present multi-TB mass stores have sustained transfer rates of 3 to 20 MB $\mathrm{s}^{-1}$. Data output from a Tflop $\mathrm{s}^{-1}$ machine would in turn be 0.14 GB $\mathrm{s}^{-1}$ (for PPM) and 2.8 GB $\mathrm{s}^{-1}$

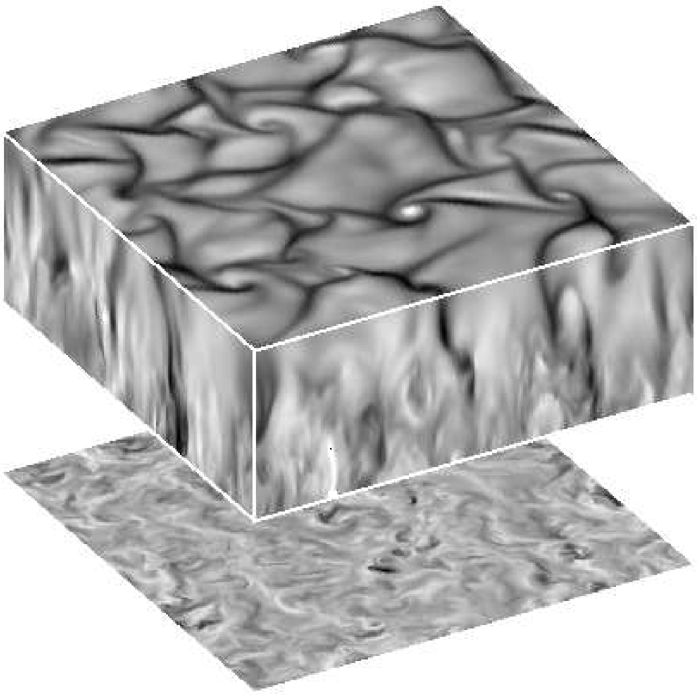

Figure 1. Perspective full domain view of vertical velocity at one instant in time in 3-D turbulent convection simulation ($256^2 \times 130$). Here $R_a = 10^7, T_a = 2{\times}10^7, P_r = 0.1$, with the rotating $f$-plane domain at latitude 45°. The rendering has upward-flowing, hot fluid as bright, with downward-flowing, cold fluid as darker tones. Note the curvaceous network at the upper surface and the smaller-scale turbulence at the bottom.

(for pseudo-spectral), or thus at worst a factor $10^3$ greater than current mass store rates. Substantial improvements in rates of data output and capture are anticipated, but it is likely that such data movement places the severest restraints on efficient simulations of turbulence. The options to help survive this looming data crunch are to sample full dumps less often, or to take compressed dumps, or used weighted averages of the data, or to do smaller problems. More acceptable is to recognize that investments must be made for data movement and capture that may turn out to be comparable in cost to that of the mpp itself.

## 3. Computational Approach

Our goals have been to first study the dynamics of increasingly turbulent states in simplified "local area" geometries with the influence of rotation incorporated via $f$–plane modelling, and then to proceed toward a more physical "global" geometry encompassing an entire rotating spherical shell of fluid. Our local-area models consist of a planar layer of fluid positioned tangentially to a rotating sphere at a latitude $\phi$. The model configuration for the fully compressible treatments is essentially that of Cattaneo et al. (1991). The physics of the model is

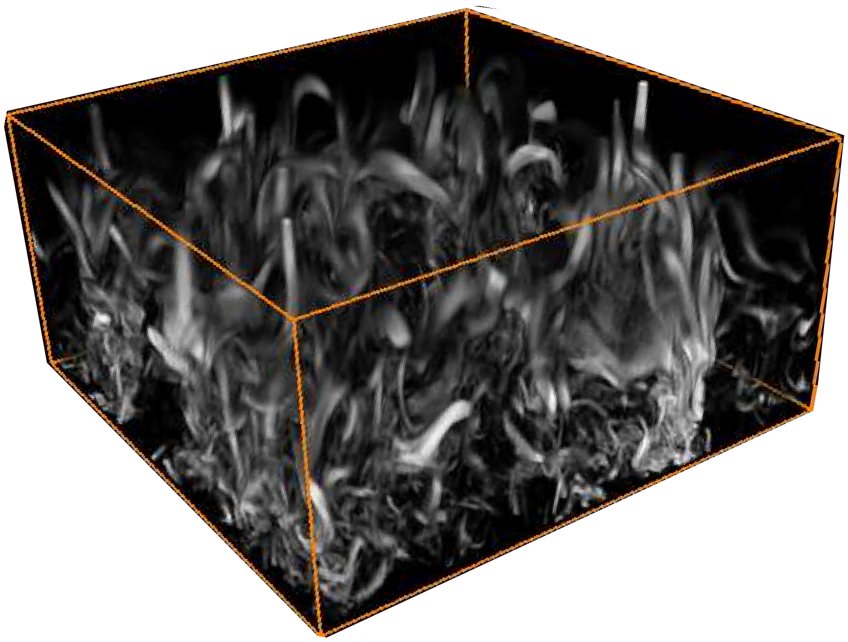

Figure 2. Perspective 3–D view of enstrophy (vorticity squared) at one instant in time as a companion to Figure 1. High enstrophy is bright and opaque whereas low enstrophy is dark and translucent. Distinctive enstrophy structures are present, with evolving cellular flows near the top of the layer yielding sheets and tubes of vorticity, whereas in the intense turbulence at greater depths the vorticity is often organized into randomly aligned tubes. Large coherent tube-like structures intermingle with small-scale random vortex tubing in the interior.

simplified by employing a perfect gas, and fluid properties such as the specific heats, shear viscosity, and thermal conductivity are also assumed constant. The flow is confined between two horizontal, impenetrable, stress-free boundaries, and the fields are assumed to be periodic in the horizontal. The upper boundary is held at a given temperature, whereas the heat flux is prescribed on the lower boundary. We then proceed to solve as an initial value problem the partial differential equations for the conservation of mass, momentum, and energy, along with the equation of state. The simulations are characterized by several nondimensional parameters: the Prandtl number $P_r$, the ratio of viscosity to thermal conductivity, the Taylor number $T_a$, the ratio of Coriolis to diffusive terms, the Rayleigh number $R_a$, the ratio of buoyancy forcing to viscous and thermal dissipation, and the Rossby number $R_o$, the ratio of nonlinear advective to Coriolis forces.

Our main computations shown here involve the solution of the fully compressible equations using a hybrid finite-difference and pseudo-spectral code. The vertical structure is treated by fourth-order finite differences in the interior. The horizontal components are treated by a pseudo-spectral method that calculates all linear operations and derivatives in spectral space $(k_x, k_y, z)$ and performs the nonlinear multiplications in configuration space $(x, y, z)$, with the transform between spaces achieved by fast transform methods. The time discretization is based on an explicit two-level Adams-Bashforth scheme, and the thermal conduction terms are treated implicitly with a Crank-Nicholson method.

## 4. Representative Results from 3–D Simulations

We have studied the basic features of fully-developed rotating compressible turbulence, with special regard to the types of flow structures, topologies, mean-flow generation, and energy balances that may be achieved. The simulations typically involve a density contrast across the layer of $\chi = 11$, spanning roughly 5 pressure scale heights. Other parameters fixed are the ratio of the specific heats, $\gamma = 5/3$, and the aspect ratio of the box, at $4:4:1$. A series of runs has been made sparsely populating the four-dimensional parameter space $(R_a, T_a, P_r, \phi)$ of the model but revealing a rich set of results. We will briefly sample some of the characteristics of such turbulent convection.

Let us first comment on the effects of rotation on the structure and topology of the turbulent convective flows. We find that convective flows in the upper thermal boundary layer consist of a nearly laminar, cellular network, atop a fully turbulent interior, punctuated by vertically-coherent structures emanating from the upper surface (e.g., Brummell, Hurlburt, & Toomre 1993, 1995a,b). There is pronounced asymmetry between the strong, narrow downdrafts and the weak, broad upflows. This is evident in Figure 1, which shows the local-area computational domain with the vertical velocity on the visible surfaces shaded according to its strength (see also Figure 5). A plane close to the lower surface of the domain has been removed to show clearly the difference in scales between the fully-developed turbulence there and the laminar upper surface. The smoothness of the upflow regions near the surface is achieved by rapid horizontal expansion of the ascending fluid elements which will tend to smooth out any small-scale fluctuations. The cell packing near the top is irregular, and cells are born and obliterated in an intricate time-dependent fashion. The Coriolis forces of rotation have changed the characteristics of both the surface network and the turbulent interior from that of earlier nonrotating models (Cattaneo et al. 1991). The surface network has become more curvaceous, less connected and more time-dependent with the addition of rotational constraints. These changes are due to inertial oscillations of surface flows induced by the underlying rotation which mobilizes the network, and to the enhancement of a mechanism for cell destruction and creation by the background pool of vorticity. In the latter, vorticity concentrated at the interstices of the downflow network lanes is amplified by the rotational influence to produce vortices which are strong enough to evacuate their interiors, thus causing a reversal of the vertical flow and the eventual destabilization of the vortex itself. These "spinners" break apart the network at the junctions and allow new upflowing cells to form there.

We find that the nature of the flows in the turbulent interior are subtly altered by rotation. The Coriolis forces provide a linear mechanism for coupling the vertical and horizontal motions, and thus with rotation the isotropy of energy and enstrophy is enhanced. This manifests itself as the concentration of vorticity into distinctive tube-like structures with a very random orientation in

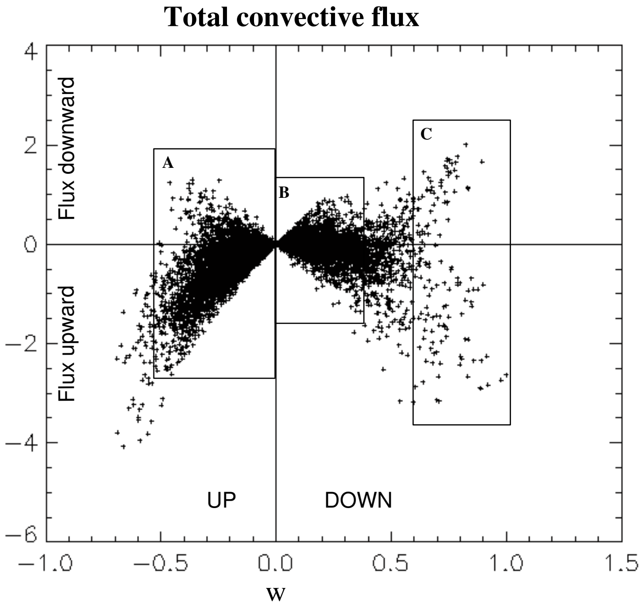


Figure 3. Phase diagram of pointwise convective flux $F_c$ as function of the vertical velocity in a horizontal plane near midlayer for turbulent convection with $R_a = 5 \times 10^5$, $T_a = 10^5$ and $P_r = 0.1$, with $R_o = 7$. The boxes A, B and C delineate horizontal sites of upflow, downflow, and strong downflow within the horizontal sampling plane.

the interior of the flow. These vortex tubes are illustrated in Figure 2, which displays the enstrophy (vorticity squared) field in a volume rendering. Near the surface, the laminar cellular flow is dominated by vortex tubes where the coherent downflows form, and by weaker sheets of vorticity generated by the downflow lanes. At greater depths, the small-scale turbulence is characterized by intricately interwoven small intense vortex tubes. Larger structures with vertical coherence are always in existence, and their presence in conjunction with Coriolis effects can lead to enhanced Reynolds stresses and thus a generation of mean flows (cf. Brummell, Xie, Toomre, & Baillie 1995). The vortex interactions of the small-scale turbulent tubes and the larger-scale vertically-coherent strong downflowing structures provide a horizontal mixing mechanism which retards the vertical mixing by the convection, yielding a mean thermal stratification in the vertical which is substantially nonadiabatic over much of the interior. This has the important and surprising consequence that with rotation, buoyancy driving of such turbulence will be experienced throughout the layer depth, and not just dominantly in the thermal boundary layers near the top and bottom of the layer.

There is a distinctive transition from laminar to turbulent flows at greater depths when the Prandtl number $P_r$ in the simulations was decreased below a value of about one-third. The flows are vigorously time dependent and turbulent, yet they exhibit coherent flow patterns recognizable over several scale heights, contrary to the assumptions of mixing-length approaches. Further, the

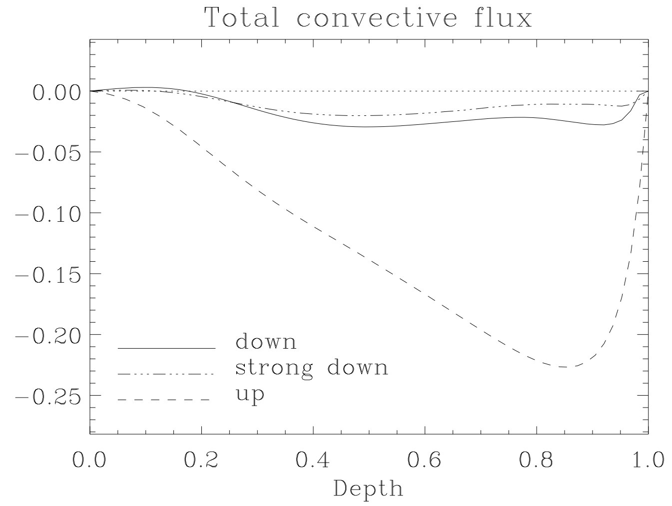


Figure 4. Horizontally-averaged convective flux $F_c$ as function of depth for the case sampled in Figure 3, revealing that the near cancellation of enthalpy and kinetic fluxes within the downflows leads to the upflows dominantly carrying the convective flux.

surface appearance of the convection, always being cellular and irregular, does not belie whether the deeper structures are laminar or turbulent. The transition to turbulence also results in remarkable changes in how the convection transports the energy. Namely, in the laminar cases the strong downflows serve to both carry most of the enthalpy flux upward and a significant kinetic energy flux downward: the upflow sites make only a modest contribution to both fluxes. However, once there is transition to turbulence at the greater depths, there is a prominent change in the role of the downflows, in which the (upward) enthalpy and (downward) kinetic flux contributions now nearly cancel each other, leaving the disorganized turbulent motions outside of those coherent structures to effect most of the overall energy transport. Thus whereas the larger scales control the convective patterns and their evolution, the transport is left to the smaller turbulent scales. This is a striking example of how transports achieved by convection can be radically modified by transitions to turbulence. Further, there are major fluctuations in the total convective flux (sum of enthalpy and kinetic fluxes) from site to site across any given horizontal plane, as the phase diagram of vertical velocity $w$ and convective flux $F_c$ in Figure 3 reveals. In the upflows (A), the pointwise $F_c$ values are sufficiently skewed that there is a net upward flux (negative) when averaged over all points, whereas the distribution is more nearly symmetrical for the moderate downflows (B) and so too for the strong downflows (C), with only a small value for the net transport emerging after averaging. This is indeed seen in Figure 4 of the horizontally-averaged $F_c$ with depth as contributed in turn by the upflows and the moderate and strong downflow regions. The contributions from the upflows dominate in the convective transport.

The results shown in Figure 4 are extraordinary, implying that throughout the turbulent layer nearly all the convective flux is carried by the upflowing ma-

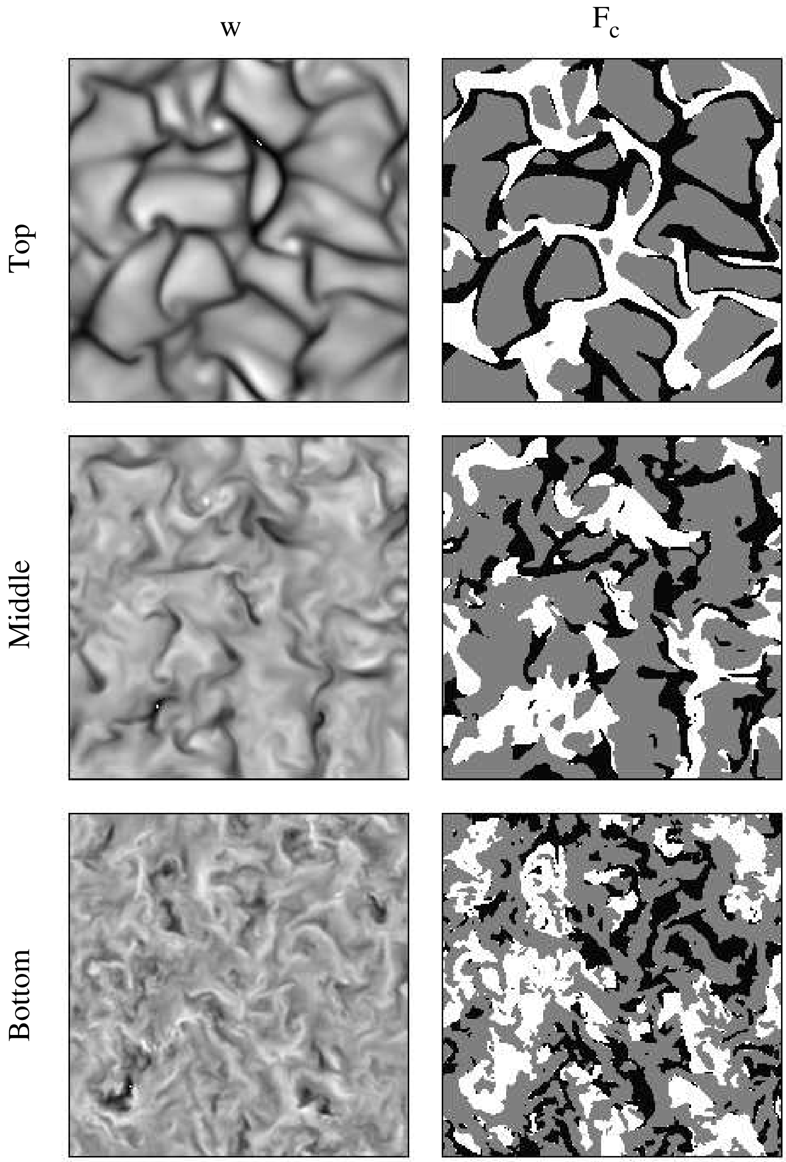


Figure 5. Vertical velocity $w$ (left) and convective flux $F_c$ (right) shown in three horizontal slices near the upper surface, middle and lower surface in single snapshot of vigorous turbulent convection for $R_a = 5 \times 10^6$, $T_a = 10^7$, $P_r = 0.1$, and $R_o = 2.24$. Upflows are lighter tones, downflows are darker tones. The change from smooth, nearly laminar flows at the top to disordered, turbulent flows deeper down is clearly evident. For $F_c$, regions of upflow are blanked out with neutral grey, and downflow regions encoded either as white or black according to the sense of $F_c$. Figure 4 indicates that horizontal averaging of these spatially intermittent fluxes in downflows leads to near cancellation.

terial and not the downflows, despite the fact that the downflows are much more coherent in space and time compared to the random fluctuations of the smaller scale upflows. The near-zero horizontal average value in the downflow at any depth is due to a cancellation of the two components of the convective flux, i.e., the enthalpy flux and the kinetic flux. Cattaneo et al. (1991) proposed a theory as to why that might be, suggesting that cancellation of the constituent fluxes at each point in the downflows is due to a Bernoulli-like balance achieved in the dynamics, provided that the motion is nearly steady, the mean stratification is nearly adiabatic, and viscous and thermal conduction are negligible. These conditions are reasonably well met in the turbulent simulations. Figure 5, however, points out that this theory may be overly simplistic. Shown is the vertical velocity and measures of the convective flux $F_c$ for three depths at a typical time in the simulation. The convective flux is shown only in the downflows (the upflows are obscured with a grey mask) with black marking regions of positive convective flux and white marking regions of negative flux. This rendering reveals that the cancellation is neither pointwise nor even local. If it conformed to the theory, then the whole downflow regions would be colored neutrally gray, or at least would have a very high frequency speckling between small black and white values. Instead, we see interleaved patches of black and white where the values of $F_c$ are actually quite large and definitely non-zero. Surprisingly, however, the horizontal average (i.e., the sum of all the black and white patches) is nearly zero. The cancellation of the convective flux appears to be more a phenomenon related to major intermittency in the flux production, both in time and space, rather than by pointwise cancellation as was first thought. These are rather subtle matters, emphasizing that highly turbulent flows can possess transport properties very different from those of laminar flows.

This work was supported in part by NSF through grant ECS–9217394 and by NASA through grants NAG5–2218 and NAG5–2256. The simulations were carried out at the Pittsburgh Supercomputer Center under grant MCA93S005P.

## References

Brummell, N. H., Hurlburt, N. E., & Toomre, J., 1993, in GONG 1992: Seismic Investigation of the Sun and Stars, ASP Conf. Ser., Vol. 42, ed. T. M. Brown (San Francisco, ASP), p. 61

Brummell, N. H., Hurlburt, N. E., & Toomre, J., 1995a,b, ApJ, submitted

Brummell, N. H., Xie, X., Toomre, J., & Baillie, C. 1995, in Proc. GONG'94, Helio- and Asteroseismology, ASP Conf. Ser., ed. R. K. Ulrich (San Francisco, ASP), in press

Cattaneo, F., Brummell, N. H., Toomre, J., Malagoli, A., & Hurlburt, N. E. 1991, ApJ, 370, 282

Gilman, P. A., & Miller, J. 1986, ApJ, 61, 585

Glatzmaier, G. A. 1987, in The Internal Solar Angular Velocity, eds. B. R. Durney & S. Sofia (Dordrecht, Reidel), p. 263

Gough, D. O., & Toomre, J. 1991, ARA&A, 29, 627